

## Coherent Electron Optics with Ballistically Coupled Quantum Point Contacts

J. Freudenfeld<sup>1</sup>, M. Geier<sup>2</sup>, V. Umansky<sup>3</sup>, P. W. Brouwer<sup>2</sup> and S. Ludwig<sup>1</sup>

<sup>1</sup>*Paul-Drude-Institut für Festkörperelektronik, Leibniz-Institut im Forschungsverbund Berlin e.V.,  
Hausvogteiplatz 5-7, 10117 Berlin, Germany*

<sup>2</sup>*Dahlem Center for Complex Quantum Systems and Physics Department, Freie Universität Berlin,  
Arnimallee 14, 14195 Berlin, Germany*

<sup>3</sup>*Weizmann Institute of Science, Rehovot 76100, Israel*



(Received 28 February 2020; accepted 7 August 2020; published 2 September 2020)

The realization of integrated quantum circuits requires precise on-chip control of charge carriers. Aiming at the coherent coupling of distant nanostructures at zero magnetic field, here we study the ballistic electron transport through two quantum point contacts (QPCs) in series in a three terminal configuration. We enhance the coupling between the QPCs by electrostatic focusing using a field effect lens. To study the emission and collection properties of QPCs in detail we combine the electrostatic focusing with magnetic deflection. Comparing our measurements with quantum mechanical and classical calculations we discuss generic features of the quantum circuit and demonstrate how the coherent and ballistic dynamics depend on the details of the QPC confinement potentials.

DOI: [10.1103/PhysRevLett.125.107701](https://doi.org/10.1103/PhysRevLett.125.107701)

Quantum point contacts (QPCs) are the smallest fundamental units of solid state based quantum circuits. These short tunable one-dimensional (1D) constrictions in a two-dimensional electron system (2DES) display an astonishingly rich spectrum of physics from the famous conductance quantization [1–3] to many-body interaction effects such as the so-called 0.7 anomaly [4–6]. Individual QPCs are important components in quantum circuits, e.g., as charge detectors [7] or to split quantum-Hall edge channels [8,9]. The complexity of QPCs has been revealed in many experiments [5] including shot noise measurements [10], scanning gate spectroscopy [11,12], thermoelectric studies [13], phototransport [14], magnetotransport out of equilibrium [15,16], or quantum transport through freely suspended devices [17]. Aspects of the ballistic dynamics of coupled QPCs have been studied in experiments focusing on non-Ohmic resistance [18–22] or magnetic deflection [15,16,23], spin-orbit coupling [24,25], defect scattering [26], or diffraction at a QPC [27]. In ballistic quantum circuits, QPCs could serve as a coherent electron source or sink. However, such a utilization requires a comprehensive understanding of the QPCs carrier emission and collection properties. Both are characterized by the coupling between the QPC's local 1D modes and the ballistic dynamics in the 2DES. Here we study the combined ballistic and coherent dynamics of two QPCs in series. Our results substantially improve our understanding of QPCs and provide a viable basis for the design of ballistic quantum circuits.

We consider two QPCs, defined electrostatically using the usual split gate design. They are tuned to their quantized conductance regimes and interact via the exchange of

ballistic electrons via a free, i.e., grounded, region of a 2DES. We demonstrate that the mutual coupling can be strongly enhanced by fine-tuning an electrostatic lens [28,29] between the two QPCs. The lens functions by refocusing carriers diverging from one QPC into the second QPC. For studying this *electrostatic focusing* we combine it with *magnetic deflection* [23,30] in a field perpendicular to the 2DES. (We avoid the common term magnetic focusing, as a homogeneous magnetic field merely deflects currents.) This combination is essential to fully determine the angular resolved emission spectrum of the QPCs and explore electrostatic focusing between QPCs. Our magnetic fields are so small that we can neglect the Zeeman splitting of electron states.

For our model calculations we first define a 2D electrostatic potential landscape based on the actual sample layout and characterization measurements. Then we determine the ballistic electron dynamics by numerically solving either the Schrödinger equation or the classical equation of motion. For our measurements we use an (Al,Ga)As/GaAs heterostructure containing a 2DES 107 nm beneath its surface. Figure 1(a) displays the surface including metal gates used to define the two QPCs and a lens in between. The 2DESs Fermi energy and mean free path measured at cryogenic temperatures are  $E_F^0 \simeq 10.9$  meV and  $l_m \simeq 24$   $\mu\text{m}$ . We performed direct current (dc) measurements in a helium-3 evaporation cryostat at  $T \simeq 250$  mK. For a basic characterization we present in Fig. 1(b) linear response pinch-off curves of the individual QPCs. The conductance as a function of gate voltages  $V_1$ ,  $V_2$  features flat plateaus at  $NG_Q$  with  $N = 1, 2, \dots$  and the spin degenerate 1D conductance quantum  $G_Q = 2e^2/h$ .

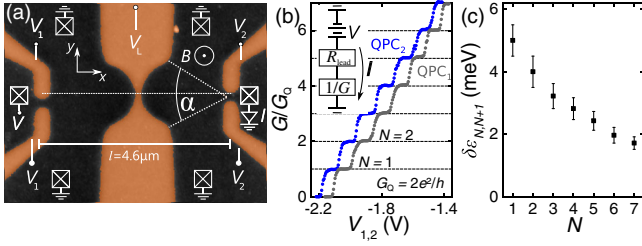


FIG. 1. (a) Atomic force microscope image of the sample; Ti/Au gates on GaAs surface (dark). Gate voltages  $V_1, V_2, V_L$  are used to define below in the 2DES QPC<sub>1,2</sub> and a lens. Source-drain voltage  $V$  is applied across QPC<sub>1</sub>; current  $I$  is measured through QPC<sub>2</sub>; the region in between is grounded via 4 Ohmic contacts (squares). The horizontal dashed line is the principal axis of the lens with aperture angle  $\alpha \simeq 55^\circ$ . (b) Individual linear response pinch-off curves  $G(V_{1,2})$  of QPC<sub>1,2</sub> ( $V_{2,1} = V_L = 0$ ), corrected for lead resistance  $R_{\text{lead}}$ . (c) Energy spacings between subsequent subbands.

The precise relation between the confinement potential of the QPCs and carrier emission profile is central for understanding the ballistic carrier dynamics and for optimizing a quantum electronic circuit. The lateral confinement defines the mode structure of the 1D channel while its potential shape in the current direction [x axis in Fig. 1(a)] governs the coupling of the 1D modes into the surrounding 2DES. Our pinch-off curves exhibit smooth steps between conductance plateaus suggesting reflectionless transmission between the free 2DES and the QPCs. This indicates smooth (parabolic) potential barriers as also implemented in our model [31]. Importantly, for reflectionless coupling the lateral 1D eigenmode structure is preserved in the coherent QPCs' emission profile.

Although the conductance steps of our QPCs in Fig. 1(b) are almost equidistant as a function of gate voltages, the corresponding energy spacings between the 1D subbands [cf. Fig. 1(c)] strongly decrease with  $N$ . These energies are incompatible with parabolic lateral confinement for  $N \geq 4$  [32]. They point to a transition by screening from a parabolic confinement for  $N \leq 1$  towards a hard wall potential for  $N \geq 4$  [33].

In the following measurements we apply a dc voltage of  $V = -1$  mV across one QPC (emitter) and measure the current  $I$  flowing to ground through the second QPC (detector), cf. Fig. 1(a). Electrons move ballistically between the QPCs as their distance of  $l \simeq 4.6 \mu\text{m}$  is smaller than  $l_m$ . Alternative current paths include backscattering through the emitter or scattering to the grounded side contacts ( $I_{\text{side}}$ ), such that the emitter current  $I_{\text{em}} = I_{\text{side}} + I$ . The resistance between the center region and ground at the side contacts is  $\simeq 37 \Omega$ , small compared to the QPC resistances exceeding  $1.8 \text{ k}\Omega$  in our measurements for  $N \leq 7$ . Nevertheless, backscattering from the macroscopic side contacts causes a small shift of the local chemical potential between the QPCs and, hence, a small

diffusive contribution to the detector current  $I$ , such that  $I = I_{\text{ball}} + I_{\text{diff}}$  with  $I_{\text{diff}} < 0.02 I_{\text{side}}$  ( $I_{\text{diff}}$  is additionally influenced by a tiny voltage offset of the current amplifier), cf. Ref. [34]. Here, we are interested in  $I_{\text{ball}}$ , the contribution to the detector current generated by carriers moving ballistically between emitter and detector.

$I_{\text{ball}}$  is limited by the divergence of the carrier modes emerging from a QPC: carriers are emitted within an aperture angle which depends on the height of the barrier in current direction and the lateral confinement along it. Given their divergence most of the carriers miss the detector and mostly contribute to  $I_{\text{side}}$ . The purpose of our lens is to refocus these carriers to enhance the coupling between the QPCs.

To first characterize the divergence and lateral mode structure of the QPCs we perform magnetic deflection experiments without electrostatic focusing [26,27]. Our QPCs are aligned in series, such that ballistic carriers emitted at a larger angle reach the detector at a higher field. In Fig. 2(a) we display example curves  $I_{N,N}$  with both QPCs tuned to the center of the  $N$ th conductance plateau with  $N = 1, \dots, 7$ . The two sets of curves correspond to opposite current directions, i.e., exchanged role of emitter vs detector. The symmetry is predicted by the Onsager relations [39] for a multiterminal device, here  $I(B)|_{\leftarrow} = I(-B)|_{\rightarrow}$ , where arrows indicate the opposite current directions [40]. Below, we will decipher the information the serial current  $I(B)$  encodes on the mode-to-mode coupling between the QPCs.

To predict  $I_{\text{ball}}$  we numerically solve the Schrödinger equation for a single electron moving in a 2D Fermi gas connected to leads as indicated in Fig. 1(a). We account for the estimated dephasing length of  $l_\phi \simeq 0.5 \mu\text{m}$  by energy averaging, where  $l_\phi$  is dominated by temperature and bias broadening. To mimic the measured mean-free path of  $l_m \simeq 24 \mu\text{m}$  we include a weak homogeneous absorbing potential between the QPCs. To model the lateral confinement of the QPCs we use a hard wall potential, where its gate voltage dependent width and depth (at the center of the constrictions) are determined from the subband spacings plotted in Fig. 1(c) [32]. The opening of the constrictions towards the leads follows the semicircular shape of the gates. The lens potential controlled by the gate voltage  $V_L$ , cf. Fig. 1(a), is added on demand. From the solution of the Schrödinger equation we extract the total transmission probability  $T_{N,M}(B, V_L) = \sum_{n,m} t_{n,m}$  of a ballistic and coherent electron through the two QPCs in series with the first (second) QPC set to the  $N$ th ( $M$ th) conductance plateau. Thereby  $t_{n,m}(B, V_L; V_1, V_2)$ ,  $n = 1, 2, \dots, N$ ,  $m = 1, 2, \dots, M$  are the transmission probabilities between the occupied transverse eigenmodes of the detector and emitter. We consider slowly varying QPC potentials and neglect coherent backreflections into the QPCs. In this limit  $t_{n,m}$  do not depend on the gate voltages for  $n \leq N$  and  $m \leq M$

and can be reconstructed from the total transmissions as  $t_{n,m} = T_{N,M} - T_{N-1,M} - T_{N,M-1} + T_{N-1,M-1}$ . The Landauer formula relates  $T_{N,M}(B, V_L)$  to the measured ballistic current,  $I_{N,M}^{\text{ball}}(B, V_L) = G_Q V T_{N,M}(B, V_L)$ .

For better illustrating the mode structure we have also measured  $I_{N,M=7}(B)$  for  $1 \leq N \leq 7$  with fixed  $M$ . Aiming at a direct comparison with model predictions we subtract the  $B$ -field independent  $I_{\text{diff}}$  from the raw data obtaining  $I_{N,M=7}^{\text{ball}}(B) = I_{N,M}(B) - I_{N,M}^{\text{diff}}(B)$  [34]. In Fig. 2(b) we plot the measured transmission differences,  $\Delta T_{N,M=7}(B) \equiv [I_{N,M=7}^{\text{ball}}(B) - I_{N-1,M=7}^{\text{ball}}(B)]/G_Q V$ , and in Fig. 2(c) as red dashed lines the bare model predictions,  $\Delta T_{N,M=7} = \sum_{m=1}^7 t_{N,m}$ . Both, measured and predicted curves display a growing magnetic field range of finite  $I_{\text{ball}}$  as  $N$  is increased. It confirms a larger aperture angle of carriers emitted from a QPC at higher modes. Our measured data roughly follow the model curves, albeit they show additional fine structure and a reduced symmetry.

So far we assumed a perfectly flat potential between two perfectly positioned QPCs. The blue solid lines in Fig. 2(c) are the result of a more realistic model taking into account the following imperfections of the sample: (i) Both QPCs are slightly shifted with respect to each other and the principal axis of the lens, cf. Fig. 1(a). These lateral shifts break the symmetry, such that  $I(B) \neq I(-B)$  similar as in our measurements in Fig. 2(b). (ii) The electrostatic potential beneath the lens is not flat but develops a dip independently of  $V_L$ . The dip is caused by the piezoelectric effect of (Al,Ga)As, which is strained by the lens gate during cool-down [34]. The combination of (i) and (ii) results in additional features in  $I(B)$  similar to our

experimental observations, albeit the agreement is not perfect: Compared to our model our measurements in Fig. 2(b) show for  $N \lesssim 5$  enhanced transmission for the outermost maxima (at larger  $|B|$ ). This is also visible as an almost bimodal current distribution in Fig. 2(a). We attribute the differences to the scattering properties of the electrostatic potential dip, visualized in Fig. 14 in Ref. [34]. Not knowing its detailed shape we assume a parabolic dip with smooth edges. Compared to our measurements it slightly underestimates the reduction of  $I^{\text{ball}}$  at  $B = 0$ . Such deviations between theory and experiment illustrate our limited knowledge of the exact potential landscape. More accurate predictions might be reached with self-consistent calculations solving the 3D Poisson and Schrödinger equations, which is beyond the scope of this article.

Next we focus on the interference pattern of the transmission curves  $\Delta T_{N,M=7}$ , which express the lateral coherence in our setup. The  $N$  maxima of each fully coherent model curve [red dashed lines in Fig. 2(c)] reflect the order of the lateral eigenmodes. A classical calculation without disorder [34] reproduces the widths and heights of  $\Delta T_{N,M}(B)$  in Fig. 2(c) but predicts a smooth transmission maximum without oscillations. The dashed gray lines in Fig. 2(c) and a copied version in Fig. 2(b) are guides to the eye. They are chosen to connect the  $n$ th maxima for odd (even)  $N$  for the bare model in Fig. 2(c). They also cut through the respective minima for even (odd)  $N$ , a fingerprint of the coherent mode structure. The measured data in Fig. 2(b) approximately reproduce the alternation between minima and maxima found in our model

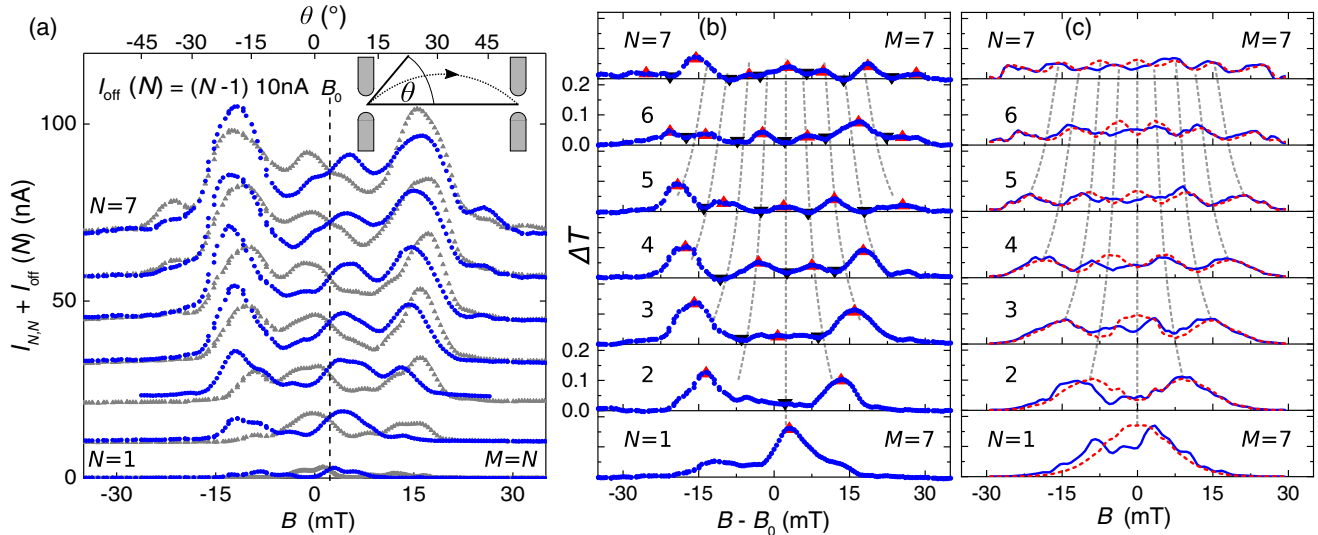


FIG. 2. (a) Magnetic deflection with two QPCs in series: measured detector current  $I_{N,N}$  versus perpendicular magnetic field  $B$  for both QPCs tuned to the  $N$ th conductance plateau with  $N = 1, \dots, 7$ . Two data sets (gray, blue) correspond to opposite current directions; vertical shifts  $I_{\text{off}}(N)$  for clarity. Measured in (b) versus calculated in (c) transmission differences  $\Delta T_{N,M=7}$ . Model curves in (c) for perfect symmetry and zero lens potential (red dashed) and with corrections of the QPC positions and accounting for the piezoelectric dip of the lens potential (solid blue lines). Maxima and minima of  $\Delta T_{N,M=7}$  are marked in panel (b) with red (black) triangles. Dashed gray lines [identical in (b) and (c)] connect the  $n$ th maxima for odd (even)  $N$  and the  $n$ th minima for even (odd)  $N$ .

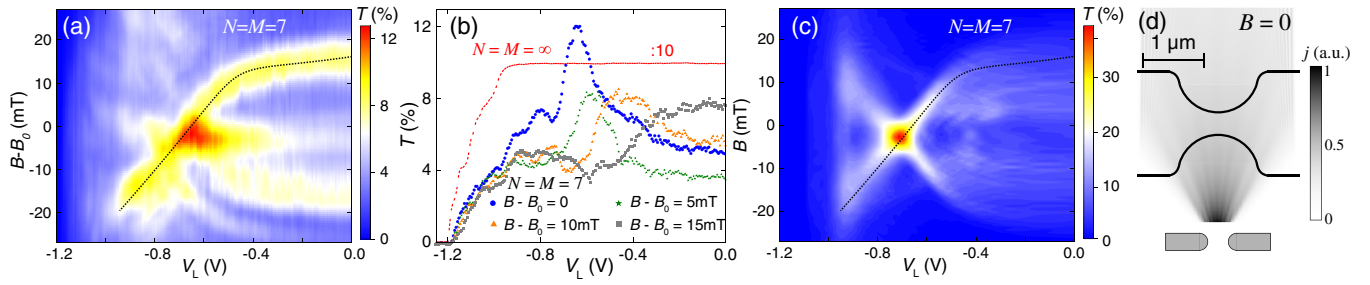


FIG. 3. (a) Measured serial transmission through both QPCs,  $T(V_L, B)$  for  $N = M = 7$  and QPC<sub>1</sub> as emitter. (b)  $T(V_L)$  for various magnetic fields. For  $B - B_0 = 0$  (blue) a pronounced maximum indicates focusing. Red dashed line:  $T(V_L)/10$  without QPCs ( $V_1 = V_2 = 0$ ). (c) Calculated  $T(V_L, B)$  as described in the main text. The dashed lines in (a) and (c) are identical. (d) Calculated current density emitted by QPC<sub>1</sub> modeled as a hard wall potential for  $N = 7$  at  $B = 0$  and  $V_L = 0$  and neglecting the electrostatic potential dip at the lens waist. Solid lines: approximate extension of the lens potential for  $V_L \simeq -0.64$  V.

calculations. The comparison confirms the coherent nature of the measured interference pattern [41].

For practical applications it is desirable to maximize the coupling of distant nanodevices, e.g., by refocusing carriers emitted from one QPC to the other. To achieve electrostatic focusing, we add a concave spherical lens in the center between the two QPCs, cf. Fig. 1(a) [28,29]. In a classical model with perfect geometry its focusing properties are described by the electronic version of Snell's law with the refractive index for electrons,  $n_r = \sqrt{E_F^0/E_F^L}$ , where the Fermi energies below the lens gate,  $E_F^L$ , and elsewhere,  $E_F^0$ , are assumed to be constants. For our concave lens focusing requires  $n_r > 1$ , i.e.  $E_F^L < E_F^0$ , which we achieve by applying  $V_L < 0$ . In Fig. 3(a) we combine electrostatic focusing and magnetic deflection and plot the measured transmission  $T(B, V_L) = I(B, V_L)/GV$  for  $N = M = 7$ . (The magnetic deflection experiment shown as gray symbols in Fig. 2(a) corresponds to the vertical cross section at  $V_L = 0$ .) While we decrease  $V_L < 0$  the current maxima bend inwards and eventually cumulate in a single peak at  $B = 0$  and  $V_L \simeq -0.64$  V, a *direct signature of electrostatic focusing*. Figure 3(b) presents various horizontal cuts  $T(V_L)$  for constant  $B$ . Independent of  $B$  the lens pinches off near  $V_L = -1.2$  V similar as the lens' transmission curve without QPCs ( $V_1 = V_2 = 0$ ), added as a red dashed line. Interestingly, the transmission maxima all lie within the range of  $V_L$  in which the lens itself causes virtually no reflection, corroborating our interpretation in terms of electrostatic focusing.

While we measure electrostatic focusing as a function of  $V_L$ , model calculations are performed in terms of the electrostatic lens potential parameterized by  $n_r$  or  $E_F^L$ . A direct comparison therefore requires a calibration of  $n_r(V_L)$ . We combined two complementary methods, namely Landau-level reflection measurements [42] and a self-consistent approach based on Snell's law [34]. The calibration allows us to display our model calculations in Fig. 3(c) in the same coordinate system as the measurements in panel (a). The dashed lines in Figs. 3(a) and 3(c) are identical and serve as a guide for comparison.

The model calculations clearly reproduce the main features of our measurements.

Figure 3(d) shows the calculated current density emitted by a QPC for  $N = 7$  at  $B = 0$  into a flat 2DES together with the actual lens geometry. It confirms that the lens captures the emitted beam for  $N \leq 7$ , in agreement with the focusing results plotted in Fig. 3(a). In Ref. [34] we show that the emission of a QPC depends on the shape of its confinement potential and that a parabolic confinement is in disagreement with our experiment.

For  $N = 7$  our model predicts a transmission at the focal point of  $T \simeq 35\%$ . About half of the reduction from 100% is caused by the discussed imperfections of the layout. The other half is due to an additional lens aberration incorporated by design: we optimized the lens for  $N = 1$  and thereby neglected the effects of bent electron beams (in contrast to straight beams in ray optics). For a bent beam the lens' focus point depends on the curvature at which carriers are emitted from a QPC. The measured transmission at the focal point is  $T \simeq 13\%$ . This further reduction indicates additional deviations of the electrostatic potential from the simulated geometry not yet accounted for in our model.

In summary, using a field effect lens we have achieved electrostatic focusing of ballistic electrons at  $B = 0$  between two QPCs separated by a mesoscopic region of grounded 2DES. As a tool to directly illustrate electrostatic focusing and to characterize the coherent lateral mode structure of the beam emitted by a QPC, we have combined electrostatic focusing with magnetic deflection. The emission profile of a QPC crucially depends on the shape of its electrostatic (confinement) potential. We present a single-particle quantum-mechanical model which provides realistic predictions of the coherent and ballistic electron dynamics for a given electrostatic potential landscape. The quality of its prediction depends on the accurate knowledge of the electrostatic potential. Atomic force and electron beam microscopy allow a precise determination of gate geometries. For the calibration of individual potential components (QPCs and lens) we apply (magneto) transport

spectroscopy. Finally, comparison of the measured and calculated current profiles  $I(B, V_L)$  through both QPCs in series allows us to extract further information on the electrostatic potential landscape such as the dip at the lens waist or details of the QPC confinement potentials. The accurate description of ballistic electrons will be key for designing future integrated quantum circuits with multiple components. Our results and methods (in experiments and theory) present an important step towards this goal.

We thank Sergey Platonov and Philipp Altpeter for technical support, Sergey Platonov and Yukihiko Takagaki for helpful discussions, and we are grateful for financial support from the Deutsche Forschungsgemeinschaft DFG via Grant No. LU 819/11-1. M. G. acknowledges support by the DFG in the framework of project A03 of the Collaborative Research Center Transregio 183 Entangled States of Matter.

J. F. and M. G. contributed equally to this work.

- 
- [1] R. Landauer, Can a length of perfect conductor have a resistance? *Phys. Lett.* **85A**, 91 (1981).
- [2] B. J. van Wees, H. van Houten, C. W. J. Beenakker, J. G. Williamson, L. P. Kouwenhoven, D. van der Marel, and C. T. Foxon, Quantized Conductance of Point Contacts in a Two-Dimensional Electron Gas, *Phys. Rev. Lett.* **60**, 848 (1988).
- [3] D. A. Wharam, T. J. Thornton, R. Newbury, M. Pepper, H. Ahmed, J. E. F. Frost, D. G. Hasko, D. C. Peacock, D. A. Ritchie, and G. A. C. Jones, One-dimensional transport and the quantisation of the ballistic resistance, *J. Phys. C* **21**, L209 (1988).
- [4] A. M. Lunde, A. De Martino, A. Schulz, R. Egger, and K. Flensberg, Electron-electron interaction effects in quantum point contacts, *New J. Phys.* **11**, 023031 (2009).
- [5] A. P. Micolich, What lurks below the last plateau: experimental studies of the  $0.7 \times 2e^2/h$  conductance anomaly in one-dimensional systems, *J. Phys. Condens. Matter* **23**, 443201 (2011).
- [6] F. Bauer, J. Heyder, E. Schubert, D. Borowsky, D. Taubert, B. Bruognolo, D. Schuh, W. Wegscheider, J. von Delft, and S. Ludwig, Microscopic origin of the ‘0.7-anomaly’ in quantum point contacts, *Nature (London)* **501**, 73 (2013).
- [7] M. Field, C. G. Smith, M. Pepper, D. A. Ritchie, J. E. F. Frost, G. A. C. Jones, and D. G. Hasko, Measurements of Coulomb blockade with a noninvasive voltage probe, *Phys. Rev. Lett.* **70**, 1311 (1993).
- [8] J. Yang, Y. Chung, D. Sprinzak, M. Heiblum, D. Mahalu, and H. Shtrikman, An electronic Mach-Zehnder interferometer, *Nature (London)* **422**, 415 (2003).
- [9] M. G. Prokudina, S. Ludwig, V. Pellegrini, L. Sorba, G. Biasiol, and V. S. Khrapai, Tunable Nonequilibrium Luttinger Liquid Based on Counterpropagating Edge Channels, *Phys. Rev. Lett.* **112**, 216402 (2014).
- [10] M. Hashisaka, Y. Yamauchi, S. Nakamura, S. Kasai, K. Kobayashi, and T. Ono, Measurement for quantum shot noise in a quantum point contact at low temperatures, *J. Phys. Conf. Ser.* **109**, 012013 (2008).
- [11] M. A. Topinka, B. J. LeRoy, S. E. J. Shaw, E. J. Heller, R. M. Westervelt, K. D. Maranowski, and A. C. Gossard, Imaging coherent electron flow from a quantum point contact, *Science* **289**, 2323 (2000).
- [12] B. Brun, F. Martins, S. Faniel, B. Hackens, G. Bachelier, A. Cavanna, C. Ulysse, A. Ouerghi, U. Gennser, D. Maily *et al.*, Wigner and Kondo physics in quantum point contacts revealed by scanning gate microscopy, *Nat. Commun.* **5**, 4290 (2014).
- [13] H. van Houten, L. W. Molenkamp, C. W. J. Beenakker, and C. T. Foxon, Thermo-electric properties of quantum point contacts, *Semicond. Sci. Technol.* **7**, B215 (1992).
- [14] C. Rossler, K.-D. Hof, S. Manus, S. Ludwig, J. P. Kotthaus, J. Simon, A. W. Holleitner, D. Schuh, and W. Wegscheider, Optically induced transport properties of freely suspended semiconductor submicron channels, *Appl. Phys. Lett.* **93**, 071107 (2008).
- [15] J. G. Williamson, H. van Houten, C. W. J. Beenakker, M. E. I. Broekaart, L. I. A. Spendeler, B. J. van Wees, and C. T. Foxon, Hot-electron spectrometry with quantum point contacts, *Phys. Rev. B* **41**, 1207 (1990).
- [16] T.-M. Chen, M. Pepper, I. Farrer, D. A. Ritchie, and G. A. C. Jones, Magnetic focusing with quantum point contacts in the non-equilibrium transport regime, *Appl. Phys. Lett.* **103**, 093503 (2013).
- [17] C. Rössler, M. Herz, M. Bichler, and S. Ludwig, Freely suspended quantum point contacts, *Solid State Commun.* **150**, 861 (2010).
- [18] P. H. Beton, B. R. Snell, P. C. Main, A. Neves, J. R. Owers-Bradley, L. Eaves, M. Henini, O. H. Hughes, S. P. Beaumont, and C. D. W. Wilkinson, The resistance of two quantum point contacts in series, *J. Phys. Condens. Matter* **1**, 7505 (1989).
- [19] D. A. Wharam, M. Pepper, H. Ahmed, J. E. F. Frost, D. G. Hasko, D. C. Peacock, D. A. Ritchie, and G. A. C. Jones, Addition of the one-dimensional quantised ballistic resistance, *J. Phys. C* **21**, L887 (1988).
- [20] L. P. Kouwenhoven, B. J. van Wees, W. Kool, C. J. P. M. Harmans, A. A. M. Staring, and C. T. Foxon, Transition from Ohmic to adiabatic transport in quantum point contacts in series, *Phys. Rev. B* **40**, 8083 (1989).
- [21] P. Coleridge, R. Taylor, A. Sachrajda, and J. Adams, Anti-collimation of ballistic electrons by a potential barrier, *Surf. Sci.* **305**, 448 (1994).
- [22] K. Liu, H. Lin, V. Umansky, and S. Hsu, Carrier density dependent electric transport of serially connected two quantum point contacts, *Physica (Amsterdam)* **42E**, 1122 (2010).
- [23] H. van Houten, C. W. J. Beenakker, J. G. Williamson, M. E. I. Broekaart, P. H. M. van Loosdrecht, B. J. van Wees, J. E. Mooij, C. T. Foxon, and J. J. Harris, Coherent electron focusing with quantum point contacts in a two-dimensional electron gas, *Phys. Rev. B* **39**, 8556 (1989).
- [24] S. Chesi, G. F. Giuliani, L. P. Rokhinson, L. N. Pfeiffer, and K. W. West, Anomalous Spin-Resolved Point-Contact Transmission of Holes due to Cubic Rashba Spin-Orbit Coupling, *Phys. Rev. Lett.* **106**, 236601 (2011).
- [25] S.-T. Lo, C.-H. Chen, J.-C. Fan, L. W. Smith, G. L. Creeth, C.-W. Chang, M. Pepper, J. P. Griffiths, I. Farrer, H. E. Beere *et al.*, Controlled spatial separation of spins and

- coherent dynamics in spin-orbit-coupled nanostructures, *Nat. Commun.* **8**, 15997 (2017).
- [26] J. J. Koonen, H. Buhmann, and L. W. Molenkamp, Probing the Potential Landscape Inside a Two-Dimensional Electron Gas, *Phys. Rev. Lett.* **84**, 2473 (2000).
- [27] P. Khatua, B. Bansal, and D. Shahar, Single-Slit Electron Diffraction with Aharonov-Bohm Phase: Feynman's Thought Experiment with Quantum Point Contacts, *Phys. Rev. Lett.* **112**, 010403 (2014).
- [28] U. Sivan, M. Heiblum, C. P. Umbach, and H. Shtrikman, Electrostatic electron lens in the ballistic regime, *Phys. Rev. B* **41**, 7937 (1990).
- [29] J. Spector, H. L. Stormer, K. W. Baldwin, L. N. Pfeiffer, and K. W. West, Electron focusing in two-dimensional systems by means of an electrostatic lens, *Appl. Phys. Lett.* **56**, 1290 (1990).
- [30] V. S. Tsoi, Focusing of electrons in a metal by a transverse magnetic field, *JETP Lett.* **19**, 70 (1974), [http://www.jetpletters.ac.ru/ps/1772/article\\_26958.shtml](http://www.jetpletters.ac.ru/ps/1772/article_26958.shtml).
- [31] J. Heyder, F. Bauer, E. Schubert, D. Borowsky, D. Schuh, W. Wegscheider, J. von Delft, and S. Ludwig, Relation between the 0.7 anomaly and the Kondo effect: Geometric crossover between a quantum point contact and a Kondo quantum dot, *Phys. Rev. B* **92**, 195401 (2015).
- [32] M. Geier, J. Freudenfeld, J. T. Silva, V. Umansky, D. Reuter, A. D. Wieck, P. W. Brouwer, and S. Ludwig, Electrostatic potential shape of gate-defined quantum point contacts, *Phys. Rev. B* **101**, 165429 (2020).
- [33] S. Laux, D. Frank, and F. Stern, Quasi-one-dimensional electron states in a split-gate GaAs/AlGaAs heterostructure, *Surf. Sci.* **196**, 101 (1988).
- [34] See Supplemental Material at <http://link.aps.org/supplemental/10.1103/PhysRevLett.125.107701> for details, which includes Refs. [35–38].
- [35] P. M. Asbeck, C.-P. Lee, and M. F. Chang, Piezoelectric effects in GaAs FET's and their role in orientation-dependent device characteristics, *IEEE Trans. Electron Devices* **31**, 1377 (1984).
- [36] T. Tanaka, H. Furukawa, and D. Ueda, A GaAs power FET with zero-temperature-coefficient, in *International Electron Devices Meeting. IEDM Technical Digest* (1997), pp. 557–560, <https://ieeexplore.ieee.org/document/650447?isnumber=14153&arnumber=650447>.
- [37] M. Büttiker, Absence of backscattering in the quantum Hall effect in multiprobe conductors, *Phys. Rev. B* **38**, 9375 (1988).
- [38] R. J. Haug, A. H. MacDonald, P. Streda, and K. von Klitzing, Quantized Multichannel Magnetotransport through a Barrier in Two Dimensions, *Phys. Rev. Lett.* **61**, 2797 (1988).
- [39] H. B. G. Casimir, On onsager's principle of microscopic reversibility, *Rev. Mod. Phys.* **17**, 343 (1945).
- [40] An offset of the symmetry point (vertical dashed line) is caused by the perpendicular component of a small residual field of  $B_0 \simeq 2.57$  mT originating from magnetized connector pins nearby the sample. Deviations from  $I(B)|_{\leftarrow} = I(-B)|_{\rightarrow}$  can be attributed to the in-plane component of the residual field or magnetic impurities.
- [41] Disorder scattering could be considered as an alternative explanation for the observed oscillations. However, to describe our measurements, this would require different arrangements of impurities for each  $N$ ,  $M$ , an unrealistic scenario.
- [42] D. Taubert, C. Tomaras, G. J. Schinner, H. P. Tranitz, W. Wegscheider, S. Kehrein, and S. Ludwig, Relaxation of hot electrons in a degenerate two-dimensional electron system: Transition to one-dimensional scattering, *Phys. Rev. B* **83**, 235404 (2011).